Implications of dust minerals on radiative transfer at regional scale, using the METAL-WRF model.

Christos Spyrou[1], Ilias Fountoulakis[1], Stavros Solomos[1], Nikolaos Papadimitriou[1,2], Alkiviadis Bais[3],
Julian Groebner[4], Daniela Meloni[5], Christos Zerefos[1,6,7,8]

[1] Research Centre for Atmospheric Physics and Climatology, Academy of Athens, 10679 Athens, Greece
[2] Department of Physics, University of Patras, Patras, Greece
[3] Laboratory of Atmospheric Physics, Aristotle University of Thessaloniki, Thessaloniki 54124, Greece
[4] Physikalisch-Meteorologisches Observatorium Davos, World Radiation Center (PMOD/WRC), Davos Dorf, Switzerland
[5] Laboratory for Models and Measurements for Air Quality and Climate Observations, ENEA, 00123, S. Maria di Galeria, Rome, Italy
[6] Biomedical Research Foundation of the Academy of Athens, Athens, Greece
[7] Navarino Environmental Observatory (N.E.O.), Costa Navarino, Messinia, Greece
[8] Mariolopoulos-Kanaginis Foundation for the Environmental Sciences, Athens, Greece

Correspondence to: Christos Spyrou (cspyrou@academyofathens.gr)

Abstract.

Dust particles originating from desert areas of the planet have significant radiative impacts on the ground and atmospheric column, changing the energy distribution of the entire earth system, which cannot be underestimated, as dust is considered a climatic regulator. The magnitude of the dust radiative effect is dependent on the optical properties of desert dust aerosols, which in turn is regulated by the composition and mineralogical content of desert dust plumes. The mineralogical composition in atmospheric models is commonly related to the soil type at dust sources and the optical properties needed are provided by observational campaigns and dedicated measurements. In this work we upgrade the METAL-WRF model to incorporate the direct radiative impact of the minerals in dust and test the impact of the direct radiative feedback on a 2-month simulation period, namely March and April 2022, when consecutive intense dust outbursts affected the Mediterranean Basin. The simulation results were compared against Global Horizontal Irradiance data and AERONET optical properties that were measured at five sites. An improvement was observed in all sites, especially close to the sources, when the minerals and dust are treated as interacting in the radiative transfer calculations, thus improving the capabilities of METAL-WRF to simulate the chemical composition of dust particles in the atmosphere along with their contribution to radiative transfer processes.

1 Introduction

Natural dust aerosols are soil particles originating from arid and semi-arid areas of the globe and they impact the climate system by changing the radiation budget of the atmospheric column, cloud formation, precipitation and marine and terrestrial biological cycles (Prospero et al., 2002; Levin et al., 2007; Solomos et al., 2011; Spyrou et al., 2013; Creamean et al., 2013;

Kallos et al., 2014; Ito et al., 2016; Spyrou, 2018; Kok et al., 2023). At high concentrations, dust particles have also considerable implications on human health (Mitsakou et al., 2008; Esmaeil et al., 2014). The magnitude of the links and feedbacks between desert dust particles and the earth system is dependent on the physiochemical properties of the aerosols at the dust source areas and on their mineralogical composition (Li et al., 2021; Solomos et al., 2023).

By modifying the radiative forcing on the ground as well as the heating rates along the atmospheric column, the dust aerosols affect the local atmospheric parameters and specifically temperature, cloud formation and precipitation due to atmospheric energy redistribution (Spyrou et al. 2010; Rap et al. 2013; Liu et al. 2014; Spyrou 2018). Dust is among the most significant factors impacting global climate, and yet there are large gaps in our knowledge regarding its interactions with solar radiation (Adeyemi et al., 2020; Li et al., 2021). Over the deserts and arid regions, as well as over regions that are in their proximity, the effect of dust on the levels of surface solar radiation is comparable to, or even dominant over, the effect of cloudiness (Derimian et al., 2006; Chen et al., 2017; Gkikas et al., 2018). As a result, the role of dust in these areas is particularly important for the regional climate, as well as for solar radiation related processes and applications,. For example, dust is the main atmospheric regulator for the levels of surface solar radiation, and subsequently for energy production from photovoltaic systems in South Mediterranean countries (Kosmopoulos et al., 2018), due to their proximity to the Saharan Desert. As we move towards higher latitudes, for instance at the north parts of Mediterranean and Central Europe, the concentration of dust in the aerosol mixture varies spatially and temporally, however its role regarding the regulation of surface solar radiation remains very significant, and occasionally more significant than the effect of cloudiness (e.g., Fountoulakis et al., 2021; Papachristopoulou et al., 2022). The mineralogical composition of dust particles affects the magnitude and spatiotemporal variability of their direct radiative impact (Scanza et al., 2015; Li et al., 2021). For instance, the dust direct radiative effect (DRE) in several longwave bands is highly dependent on quartz, calcite and hematite content (Mishra et al., 2008). Across many shortwave bands dust DRE strongly depends on the iron-oxide content and its mixing state with other minerals in the atmosphere (Sokolik et al., 1998; Sokolik and Toon, 1999; Li et al., 2021).

The dust mineralogical composition in atmospheric models is commonly related to the soil type at dust sources, as provided by a global geological database (e.g., Claquin et al., 1999; Nickovic et al., 2013; Scanza et al., 2015).

The limited knowledge of mineral dust composition at the dust sources worldwide hinders the ability of regional and global models to provide reliable dust projections and aforementioned impacts on radiative transfer (Rodriguez-Navarro et al., 2018; Solomos et al., 2023). However, despite the underlying uncertainties, taking into account the varying composition of dust particles, improves the accuracy in modeled dust impacts (Obiso et al., 2023). Some attempts at handling the lifecycle of minerals in the atmosphere include the work by Scanza et al., 2015, who used a global soil mineralogy atlas based on Claquin et al.(1999) to simulate minerals in the Community Atmosphere Model version 4 (CAM4); Li et al.(2021) who updated the simulations for the Community Atmosphere Model version 5 (CAM5); Bergas-Massó et al., 2022 who used the Earth System Model (ESM) EC-Earth3-Iron; Gonçalves Ageitos et al., 2023 who applied the Multiscale Online Nonhydrostatic AtmospheRe CHemistry (MONARCH) model in global scale and Hamilton et al., 2019 who used the Community Earth System Model (CESM) in order to assess the emission and atmospheric processing of iron at global scale. Recently, Solomos et al., 2023

developed the METAL-WRF model as an extension to the WRF-Chem model, to include the production, transport and deposition of different minerals originating from the dust source areas.

70 Due to the inherent impact of physiological and chemical characteristics of minerals in estimating the DRE at both shortwave and longwave bands, recent attempts have been made in coupling the model radiative transfer processes with specific mineral optical properties (Scanza et al.,2015; Perlwitz et al., 2015; Li et al., 2021). In the work of Scanza et al.,2015 the authors updated the CAM4 model to include the optical properties and radiative feedback of minerals, through the use of the proper refractive indexes. However, the CAM4 model neglects scattering in the longwave, which leads to underestimation of the

75 radiative forcing. Similarly, Perlwitz et al., 2015 described the incorporation of the eight minerals in the NASA Goddard Institute for Space Studies (GISS) Earth System ModelE2 and followed closely the developments of Scanza et al., 2015, with Li et al., 2021 providing a review of the various numerical attempts in quantifying the DRE of minerals. The aforementioned studies are constrained by the use of global models, further aggravating the existing uncertainties of mineralogy datasets (Solomos et al., 2023), and an improved description of mineralogy partition in the sources is needed. This kind of information

80 is planned in the Earth Surface Mineral Dust Source Investigation (EMIT) mission, through the use of satellite data.

In this work we further update the METAL-WRF Regional Model (Solomos et al., 2023), which was specifically developed to simulate the mineral components of desert dust particles, to include the radiative impact of dust particles. The ability of the new model to accurately simulate surface solar irradiance in terms of Global Horizontal Irradiance (GHI) during dust outbreaks is evaluated over European and African sites for a two-month period when all sites were affected by several dust episodes. The

85 manuscript is organized as follows: Section 1 provides an introduction and state-of-the-art. In Section 2 we present the developments made on the framework of METAL-WRF in order to incorporate the impact of minerals on radiative forcing and the data used in this work. In Section 3 we present the sensitivity tests and results on the comparison between modelled data and station measurements and finally Section 4 contains concluding remarks of the manuscript.

2 Methodology and Data used

90 ### 2.1 Optical Properties and Model Development

A new integrated system has been developed that is able to simulate the mineral life cycle in the atmosphere and quantify the direct radiative impacts of minerals contained in dust particles. The host model is the METAL-WRF model described in Solomos et al., 2023. The system is based on the WRF (Weather Research and Forecast) model (Skamarock et al., 2021) with the ARW core (Advanced Research WRF) coupled with the chemistry module (WRF-Chem; Grell et al., 2005) which allows

95 for the representation of various chemical species and aerosols in the atmosphere, including desert dust. The dust model used is the GOCART module, with the Air Force Weather Agency (AFWA) dust emission scheme (Ginoux, 2001; LeGrand et al., 2019). For the mineralogy of desert dust, the GMINER30 dataset developed by Nickovic et al., 2012 is used. The GMINER30 is a very high-resolution global database which contains mineral fractions in potentially erodible soils and has been specifically designed to support the parameterization of mineral emissions contained in desert dust in atmospheric numerical models. The

100 database contains information on illite, kaolinite, smectite, calcite, quartz, feldspar, hematite, gypsum and phosphorus fractions, distributed over clay and silt dust populations on a 30 arc-seconds grid (Nickovic et al., 2012). The resulting system, METAL-WRF, is capable of simulating adequately the aforementioned mineral concentrations in the atmosphere and can be the basis of including the subsequent feedback of these minerals in the atmospheric column.

An important component of the WRF-chem model is the ability to handle various atmospheric species on a sectional approach,

105 as this approach connects the various WRF-Chem chemical modules with the optical properties' module, allowing for the calculation of the optical properties of mixed air layers (Barnard et al., 2010; Zaveri et al., 2008). Each constituent of the atmosphere is associated with a complex refractive index and the Mie theory (Ackerman and Toon, 1981) is used to calculate the extinction efficiency, Q_e, the scattering efficiency, Q_s, and the intermediate asymmetry factor, g, as functions of the size parameter, which is the particle's radius (Fast et al., 2006), along with the dust number density (Ukhov et al. 2021) and mineral

110 number density.. Therefore, dust and various mineral refractive indexes are needed over the entire radiation spectrum (both short and long wave radiation) to perform these calculations. For dust, the complex refractive index is set to $1.55 + 0.002i$ (Ukhov et al., 2021). For the minerals, the complex refractive indices are set using the work of Scanza et al., 2015. Illite and kaolinite values originate from Egan and Hilgeman (1979) in the shortwave and Querry (1987) in the longwave. Hematite data is acknowledged as A.H.M.J. Triaud, private communication (2005). Quartz is the average of O--ray and E--ray data from the

115 HITRAN96 dataset (Rothman et al., 1998). Calcite and Gypsum are calculated from data presented in Long et al., 1993 and feldspar refractive indices are given only for shortwave from Egan and Hilgeman, 1979. More information on the datasets used and the values implemented is presented in the supplement of Scanza et al. 2015. The mixing of dust and minerals is handled as described in Barnard et al., 2010, by using the spherical shell/core configuration (Bond et al., 2006).

Computationally the process can be described as:

120 1) The mass of each mineral is calculated at each layer. METAL-WRF calculates masses for each of the 8 minerals (kaolinite, illite, smectite, quartz, feldspar, hematite, calcite and gypsum). Additionally, we account for the mass of dust not included in the aforementioned minerals. This "dust mass" retains the complex refractive index of $1.55 + 0.002i$.

2) For each size bin the masses are converted to volumes, by dividing by the density of each mineral. The assumed densities are given in Ageitos et al., 2023 and presented here in Table 1.

125 **Table 1. Mass densities defined for each mineral in METAL-WRF**

Mineral	Density (kg/m3)
Kaolinite	2630
Illite	2570
Smectite	2570
Quartz	2670
Feldspar	2680

Hematite	5210
Calcite	2710
Gypsum	2308
Iron	4770

130

3) The size distribution of the minerals is assumed to follow the size distribution of dust, partitioned in 5 bins defined by effective radii of 0.73, 1.4, 2.4, 4.5, and 8.0 μm, corresponding to particle diameter ranges of 0-1 μm, 1-1.8 μm, 1.8-3 μm, 3-6 μm and 6-10 μm (see Solomos et al., 2023 and LeGrand et al., 2019 for more information).The refractive index of

135   the particles in each size bin is calculated by volume averaging.

4) The total refractive index of the minerals and dust is then calculated as per eq.1.

$$r_i(\lambda) = ref\_index_{dust}(\lambda) * \left(\frac{mass_{dust}}{dens_{dust}}\right) + ref_{index\,illite}(\lambda) * \left(\frac{mass_{illite}}{dens_{illite}}\right)$$

$$+ ref_{index\,kaolinite}(\lambda) * \left(\frac{mass_{kaolinite}}{dens_{kaolinite}}\right) + ref_{index\,quartz}(\lambda) * \left(\frac{mass_{quartz}}{dens_{quartz}}\right)$$

$$+ ref_{index\,calcite}(\lambda) * \left(\frac{mass_{calcite}}{dens_{calcite}}\right) + ref_{index\,hematite}(\lambda) * \left(\frac{mass_{hematite}}{dens_{hematite}}\right)$$

140

$$+ ref_{index\,gypsum}(\lambda) * \left(\frac{mass_{gypsum}}{dens_{gypsum}}\right) + ref_{index\,feldspar}(\lambda) * \left(\frac{mass_{feldspar}}{dens_{feldspar}}\right)$$

$$+ ref_{index\,smectite}(\lambda) * \left(\frac{mass_{smectite}}{dens_{smectite}}\right) + ref\_index_{iron}(\lambda) * \left(\frac{mass_{iron}}{dens_{iron}}\right) \qquad (Eq.1)$$

where $ref_{index\,i}$ is the complex refractive index of each mineral i at each wavelength λ.

5) The refractive index of dust is then treated similarly to the refractive index of the other atmospheric elements in the atmospheric column (i.e. NO_3, water vapour e.t.c) for the calculation of radiative transfer in the RRTMG radiative transfer

145   module (Iacono et al., 2008).

2.2 Experimental Design

In order to evaluate the impact of the presence of minerals in the atmospheric column, two sets of simulations have been performed using METAL-WRF: (i) One simulation where the dust and associated minerals are treated as passive tracers and do not interact with shortwave or longwave radiation (RADOFF). (ii) In the second set of simulations, the minerals are treated

150   as active in the entire radiation spectrum (RADON). The RADON simulations include only the direct and semi-direct effects of particles in the atmospheric energy distribution. The indirect aerosol impacts are omitted in this work. Then, the aerosol optical properties and the Global Horizontal Irradiation (GHI) that were retrieved from the two different sets were compared with the measurements. The METAL-WRF domain for all the simulations (along with the topography) is given in Figure 1.

The simulation domain was selected to include the entirety of the Saharan dust with the associated dust and mineral sources.
155   The various fractions for soil and silt soils are presented in Figure 2.
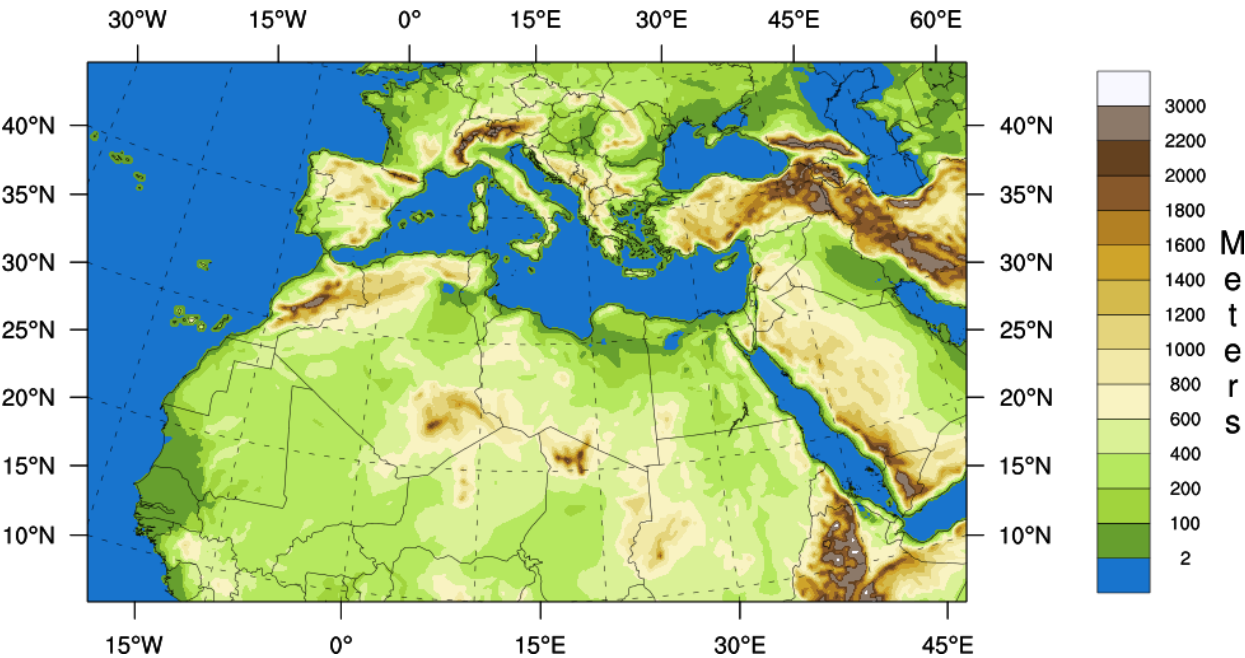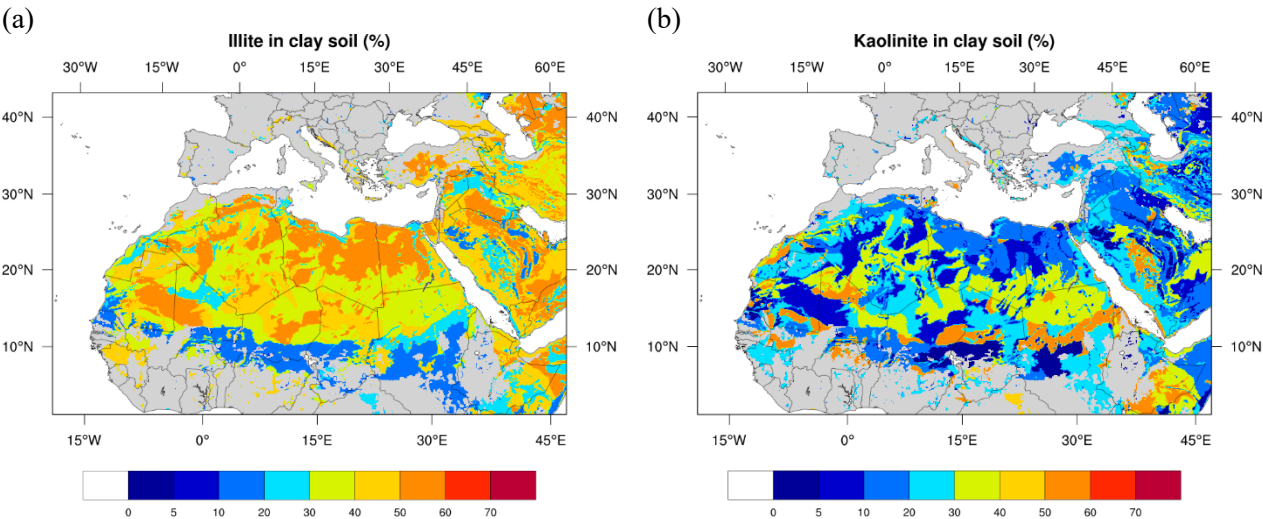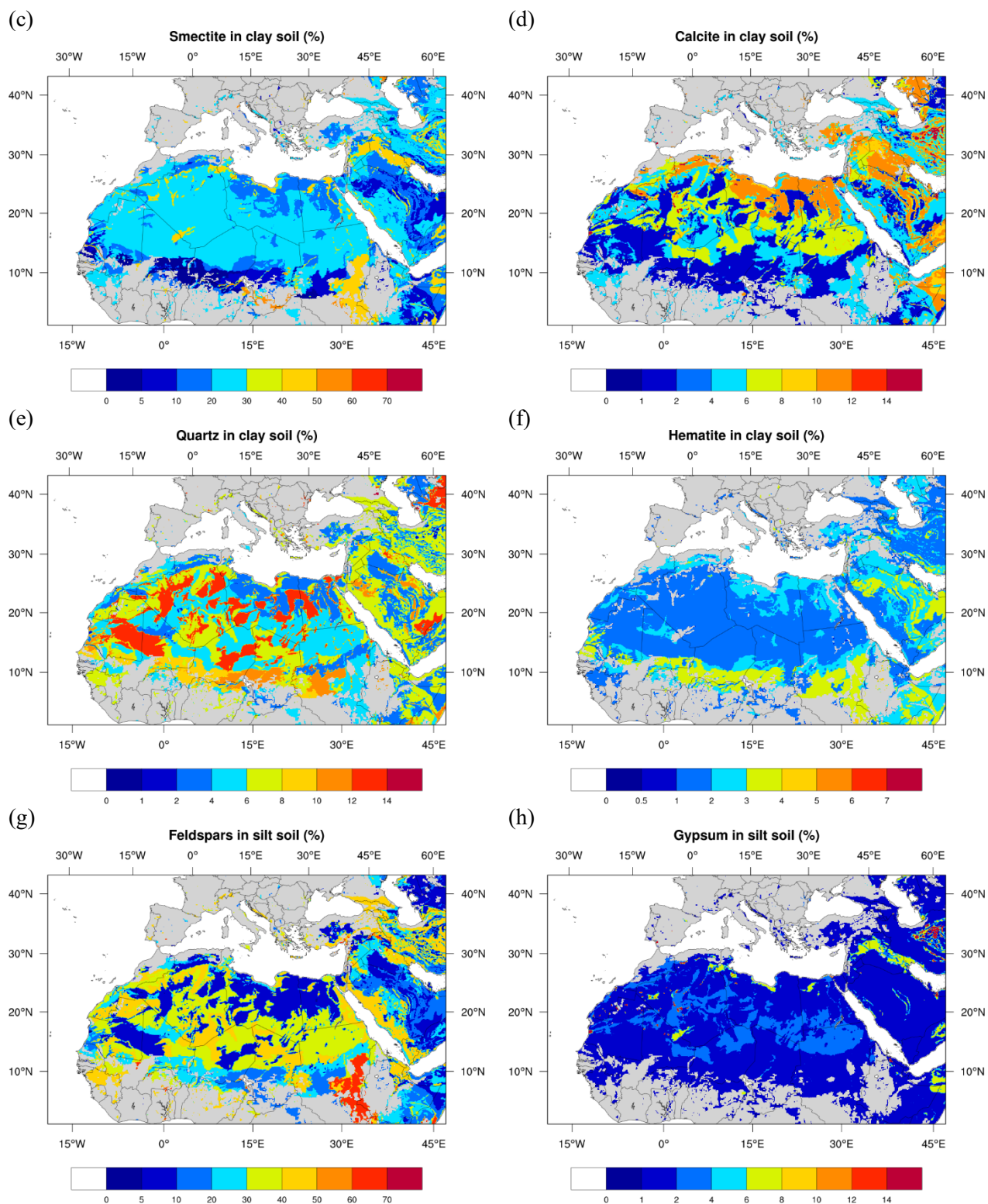

Figure 1 Domain of METAL-WRF used in the simulations. The topography in meters is also defined.

160

(a)

Illite in clay soil (%)

(b)

Kaolinite in clay soil (%)
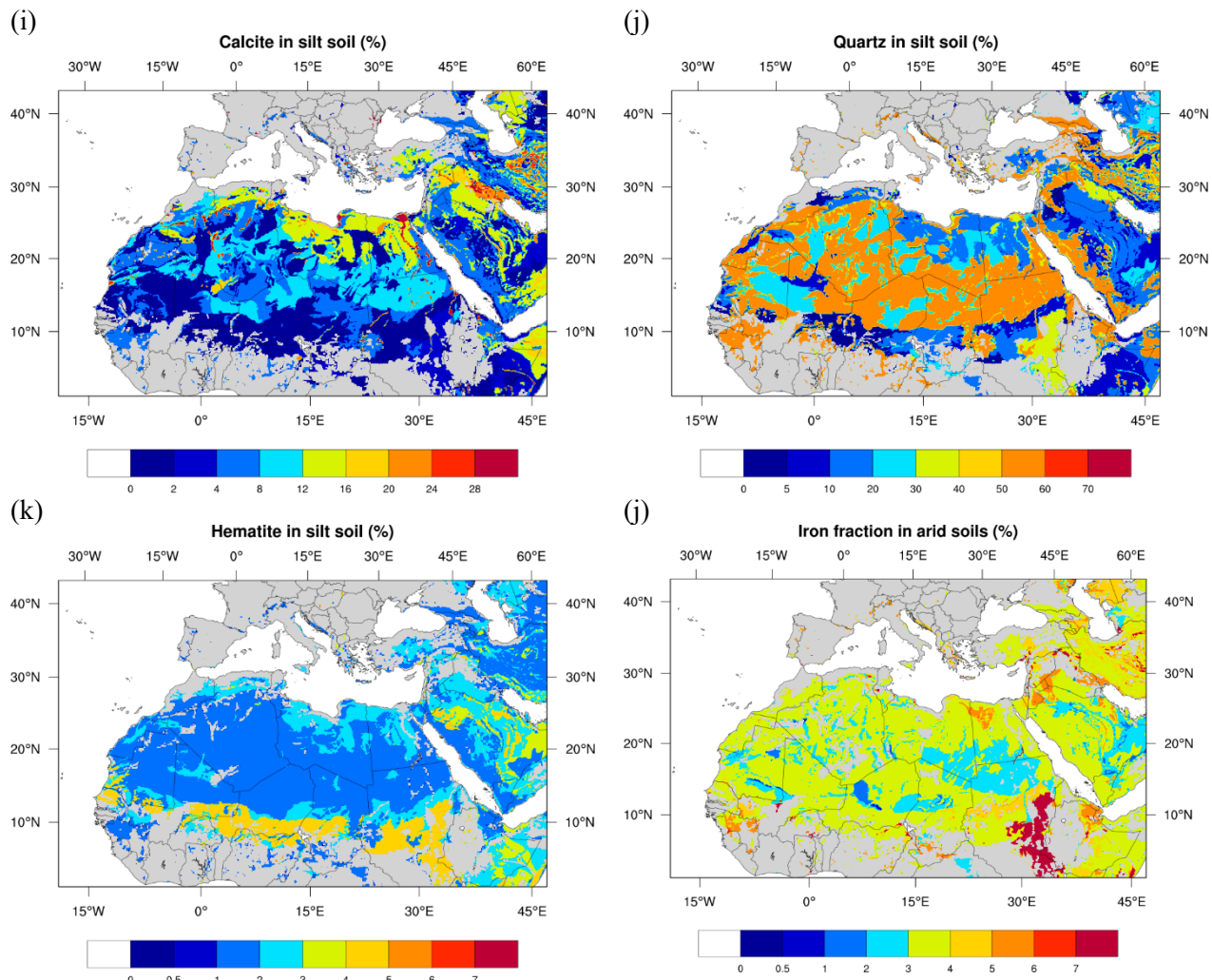
(i)

(j)

(k)

(j)

Figure 2 Mineral fractions in arid soils in the selected METAL-WRF configuration. The fractions are given for illite (a), kaolinite (b), smectite (c), calcite (d), quartz (e), hematite (f) in clay soils and feldspar (g), gypsum (h), calcite(i), quartz(j), hematite(k) and iron(i) in silt soils (source Solomos et al., 2023).

The model is set up with a resolution of 15 Km × 15 Km, with 32 vertical hybrid-sigma levels stretching from the surface to the top of the atmosphere (50hPa), a runtime timestep of 60sec and hourly outputs. The physical parameterizations used in these runs are presented in Table 2.

8

Table 2. Physical Schemes and used in the METAL-WRF setup

Parameterization	*Scheme*	*Reference*
Microphysics	Thompson Scheme	Thompson et al., 2008
Cumulus	Grell-Freitas Scheme	Grell and Freitas 2014
Shortwave/Longwave radiation	RRTMG scheme	Iacono et al., 2008
Surface Layer physics	Eta similarity scheme	Janjic, 1996; 2002
Land Surface	Noah Land Surface Model	Tewari et al., 2004
Planetary Boundary layer	Mellor-Yamada-Janjic scheme	Mesinger 1993; Janjic 1994
Dust module	GOCART simple aerosol scheme	Ginoux, 2001
Dust emission scheme	AFWA	LeGrand et al., 2019

175   The initial and boundary conditions are from the ERA5 reanalysis dataset (Hersbach et al., 2020), produced by the Copernicus Climate Change Service (C3S) at the European Centre for Medium-Range Weather Forecasts. Sea Surface Temperature analysis datasets were provided by the Copernicus Marine Environment Monitoring Service (CMEMS) at a resolution of 1/12° (GLORYS12V1 product) and updated daily in all the simulations. The use of CMEMS SST`s has been found to improve the performance of WRF model in Mediterranean simulations (Varlas et al., 2020; Spyrou et al., 2022).

180   **2.3 Ground Measurements**

To evaluate the ability of the model to simulate surface solar radiation, the Global Horizontal Irradiance (GHI) as well as key optical properties were compared with actual measurements. The ground-based datasets that were used for the comparison are discussed in the sections below. For the comparison, we choose a 2-month period (March-April 2022) when consecutive intense dust outbursts affected the Mediterranean Basin. As shown in Papetta et al. 2025 (under preparation to be submitted to

185   ACP), for specific days during this period, more than 90% of the Aerosol Optical Depth (AOD) can be attributed to the presence of desert dust particles over extended areas of the Mediterranean region.

2.3.1 GHI Measurements

The Ground-based Global Horizontal Irradiance (GHI) that was measured by pyranometers operating at five sites (see Table 3) with quite different characteristics has been used for this study. In addition to the reliable (quality assured) ground-based

190   GHI measurements, measurements of aerosol optical properties were also available at these locations and have also been used. The GHI at three of the stations (Tamanrasset, Magurele, Lampedusa) is quality assured by following the strict protocols of the Baseline Surface Radiation Network (BSRN; Driemel et al., 2018). Although Lampedusa was not member of the BSRN in 2022, the strict BSRN criteria were already followed at the station. At the stations of Davos and Thessaloniki, strict quality control/quality assurance protocols are also followed (Natsis et al., 2024), even though these sites are not BSRN members. At

195 all five sites, measurements of columnar aerosol optical properties are available from CIMEL sunphotometers that participate in the AERONET network (Holben et al., 1998; Giles et al., 2019).

The station located at Tamanrasset belongs to the National Meteorological Office of Algeria and is located in the Sahara Desert. The Lampedusa station is a remote marine site belonging to the Italian National Agency for New Technologies, Energy and Sustainable Economic Development (ENEA) and the measurements are carried out at the Lampedusa Atmospheric

200 Observatory. Due to the position of the island, relatively close to the Saharan desert, the cases of desert dust transport are frequently detected, particularly in spring and summer (Meloni et al., 2008). The urban station of Magurele, Romania is hosted at the National Institute of Research and Development for Optoelectronics (INOE). The station of Thessaloniki is located at the campus of the Aristotle University of Thessaloniki, Greece. The Thessaloniki site is a typical urban Mediterranean site. The alpine station of Davos is hosted at the facilities of the Physical Meteorological Observatory in Davos, that is part of the

205 world radiation center (PMOD/WRC).

Table 3. The five sites used for this study and their coordinates

Site	Coordinates
Tamanrasset, Algeria	22.79° N, 5.53° E, 1377 m
Thessaloniki, Greece	40.63° N, 22.96° E, 60 m
Magurele (INOE), Romania	44.35° N, 26.03° E, 90 m
Davos, Switzerland	46.81° N, 9.84° E, 1589 m
Lampedusa, Italy	35.52° N, 12.63° E, 45 m

210 For all sites, the effective altitude for which METAL-WRF provides the GHI differs by less than 100 m from the real altitude of the stations that are listed in Table 3. Thus, it is considered that any altitude differences between the model and the stations do not have a significant impact, neither on GHI, nor on aerosol optical properties.

2.3.2 AERONET optical properties

AERONET was created in the late 1990s and is currently composed of more than 600 sun-photometers (type CIMEL CE318,

215 commonly referred as CIMEL sun-photometers) that have been deployed world-wide. The CIMEL measures sun and sky radiance spectrally, at nine distinct wavelengths (340 nm, 380 nm, 440 nm, 500 nm, 675 nm, 870 nm, 940 nm, and 1020 nm). Most recent CIMEL models include one more channel (at 1640 nm). The 940 nm channel is used to retrieve columnar water vapor, while the remaining eight channels are used to retrieve aerosol optical properties (Holben et al., 1998). The direct sun measurements are used to derive spectral Aerosol Optical Depth (AOD) at the eight wavelengths, the Angstrom Exponent

220 (AE) for different wavelength couples, and the columnar water vapor (Giles et al., 2019). Sky radiance measurements are

performed for solar zenith angles 50° - 75° and are then processed using an inversion algorithm (Dubovik, 2000; Dubovik and King, 2000) to derive size distribution (SD), spectral Single Scattering Albedo (SSA), Asymmetry Parameter (ASY), and other products, that are derived either from the sky radiance measurements, or by combining direct sun and sky-radiance measurements (O' Neill et al., 2003).

225 AERONET products have been widely used for climatological studies (e.g., Holben et al., 2001; Toledano et al., 2007; Kaskaoutis et al., 2007) and satellite validation (e.g., Fan et al., 2023; Cheng et al., 2012). For this study, the AERONET version 3, level 2 (V3L2) product has been used (Giles et al., 2019, Sinyuk et al. 2020).

2.3.3 METAL-WRF calculations

METAL-WRF provides directly the GHI as calculated by the RRTMG radiative transfer algorithm (Mlawer et al., 1997; Iacono
230 et al., 2008), including also the profiles of aerosol optical properties, as described in Section 2.1. To attribute the GHI from the model to the columnar aerosol optical properties we calculated the integrals of the profiles (i.e., the AOD was calculated by integrating the vertical distribution of the extinction coefficient), and also the effective values of optical parameters. Effective Single Scattering Albedo (SSA), Asymmetry Parameter (ASY) and Angstrom Exponent (AE) have been calculated as the average of the profiles of these properties that have been weighted with the vertical distribution of the aerosol extinction
235 coefficient. For example, the effective SSA is calculated as:

$$SSA = \frac{\sum_i SSA_i \cdot ext_i}{\sum_i ext_i} \qquad \text{(Eq. 2)}$$

The effective ASY and AE have been calculated similarly as the SSA. All optical properties from the model have been calculated at 400, 500, 600, and 1000 nm.

2.3.4 Comparison between the GHI from the model and the measurements

240 To evaluate the ability of METAL-WRF to simulate the GHI for RADON (dust interacts with solar radiation) with respect to RADOFF (dust does not interact with solar radiation) we compared: (i) daily integrals of the GHI from the measurements and the model, and (ii) individual GHI measurements corresponding to the time of the model outputs (the model temporal resolution is one hour). In the latter case we tried to assess the differences in aerosol optical properties and cloudiness for the two modes, as well as the improvement in the modelled GHI when radiation interacts with dust. The optical properties that are used for
245 the analysis have been calculated as the 30-min averages (+/- 15 mins) around the time of the GHI measurements. Daily integrals were calculated when all measurements in a day were available. The results of the comparison between the daily GHI integrals are indicative for the improvements in the ability of the model to simulate daily GHI at sites that are strongly affected by dust.

For the comparison between the hourly GHI values we considered the following cases:

250   a) **Unobstructed solar disk during dust events (clear-skies):** To make data selection we considered only cases where neither the model nor AERONET consider clouds in front of the sun. Regarding ground-based measurements, we

only considered GHI values where at least four AERONET (direct sun) AOD measurements were available within the selected 30-min period. For Tamanrasset and Lampedusa we considered all cases with at least one (instead of eight) AOD measurements in an hour because at these sites many AOD measurements are filtered out (erroneously

255 considered as clouds) because of the large AOD temporal variability during intense dust events. Additionally, we only used the previously selected data when the 440 – 675 nm AE measured by the CIMEL was below 1 (i.e., large particles were dominant in the aerosol mixture). Under such conditions we can evaluate whether the addition of interactive dust chemistry (RADON) improved the modeled GHI or not, under cloudless sky conditions, during dust events (assuming that in all cases, AE<1 represents dust dominated aerosol mixtures). Obviously, even when AE<1

260 the aerosol mixture includes various aerosol species, especially at the sites that are at longer distances from the Sahara Desert, and that are also affected by local aerosol sources. Nevertheless, this study aims to evaluate whether the inclusion of dust-radiation interactions improves the model ability to simulate GHI during realistic dust events, and the extent at which it alters the properties of atmospheric constituents that affect radiative transfer processes in the atmosphere (i.e., the aerosol properties, water vapor and cloudiness) considered by the model over the different sites.

265 For the analysis we considered only cases when solar zenith angle (SZA) is below 70° (i.e., when the levels of GHI are higher, and thus errors are more significant).

b) **All-sky conditions during dust events (all-skies):** To make the data selection we considered two sub-cases: (i) dust optical depth (DOD) from the model above 0.05, and (ii) dust optical depth from the model below 0.05. The two sub-cases have been chosen to investigate (also by comparing with case a) if improved representation of the semi-direct

270 dust effect (when the model considers the presence of a non-negligible amount of dust) results in improved GHI modelling, in addition to the consideration of the interactions between dust and solar radiation.

3 Results and discussion

3.1 Comparison between daily GHI from measurements and the model

The results of the comparison between the daily GHI from the measurements and the model are presented in Figure 3 for

275 Tamanrasset. This station is selected due to its critical position inside the Saharan desert, close to the dust and mineral sources. The results for the other four sites that were described in Sect. 2 are presented in the supplement (Figures S1 – S4). The slope (a) and the intercept (b) of the linear fits that represent the relationship between the measurements and the simulations, as well as the correlation coefficient (r) are presented in Table 4. For the RADOFF simulations the model tends to overestimate the daily GHI mainly since it does not consider the interaction (scattering/absorption) of the solar radiation with dust and mineral

280 particles. Additionally, as discussed in the following sections, the effect of cloudiness is represented more accurately in RADON. In all cases, RADON results in smaller differences and a better correlation between the modelled and measured daily integrals, since the radiative links and feedbacks are taken into account in the simulations, providing a better representation of the energy distribution in the atmospheric column and the surface. The improvement is, as expected, larger over sites where

aerosol mixture is dominated by dust aerosols. Though, even at sites where many species contribute to the aerosol mixture, the
285   improvement in the agreement between the model and the measurements is clear.

The lowest correlation coefficient was found for Davos, where although it improves significantly for RADON it is still of the order of 0.4 (while for all other stations it is above 0.75), mainly because the model cannot capture accurately the variable cloudiness conditions at Davos. The biggest improvement has been found for the sites that are affected more strongly by dust (i.e., for Lampedusa and Tamanrasset). In all cases the slope of the linear fit is getting closer to unity and the intercept is getting
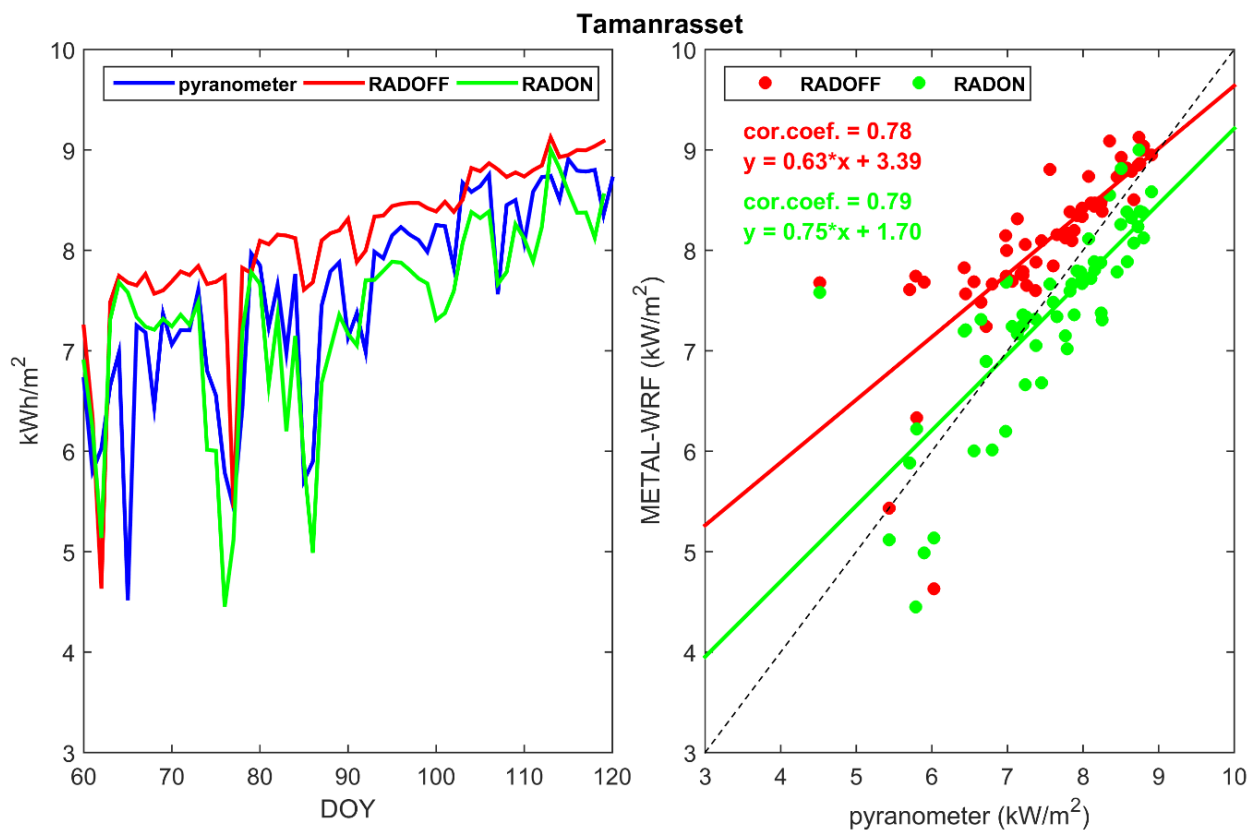290   closer to zero for RADON.

Figure 3 Left: Daily GHI with respect to the day of year (DOY) 0f 2022, as it was calculated from the pyranometer measurements (blue), the METAL-WRF RADOFF (red), and the METAL-WRF RADON (green). Right: Correlation between the daily GHI
295   **from the pyranometer and the METAL-WRF RADON (green). Right: Correlation between the daily GHI from the pyranometer and the model for RADOFF (red) and RADON (green). The results presented are for Tamanrasset.**

300

305 **Table 4 Slope (a), intercept (b), and correlation coefficient (r) of the linear fits that were used to describe the relationship between the daily GHI integrals from the measurements and the model.**

	RADOFF			RADON		
	a	b	r	a	b	r
Davos	0.29	5.01	0.29	0.35	4.04	0.38
INOE	0.70	2.19	0.85	0.74	1.74	0.86
Lampedusa	0.48	3.78	0.52	0.75	1.19	0.77
Tamanrasset	0.61	2.77	0.71	0.61	2.47	0.75
Thessaloniki	0.63	3.39	0.78	0.75	1.70	0.79

3.1 Comparison between instantaneous GHI from measurements and the model

310 **3.1.1. Clear-sky**

To estimate the extent of the improvement of the parameterization of aerosol optical properties for the RADON simulations, and how this contributes to the stronger correlation between the measured and the modeled GHI (in addition to the dust-radiation interactions), we compared the measured and modeled GHI under clear-skies (as defined in Sect. 2.3.4). The comparison between measured and modeled GHI is presented in Figure 4. The correlation coefficient is similar for RADON

315 and RADOFF for four out of the five stations, except the Davos station. However, for RADON the linear fit that describes the relationship between the measured and modeled GHI is in all cases closer to the y=x line.
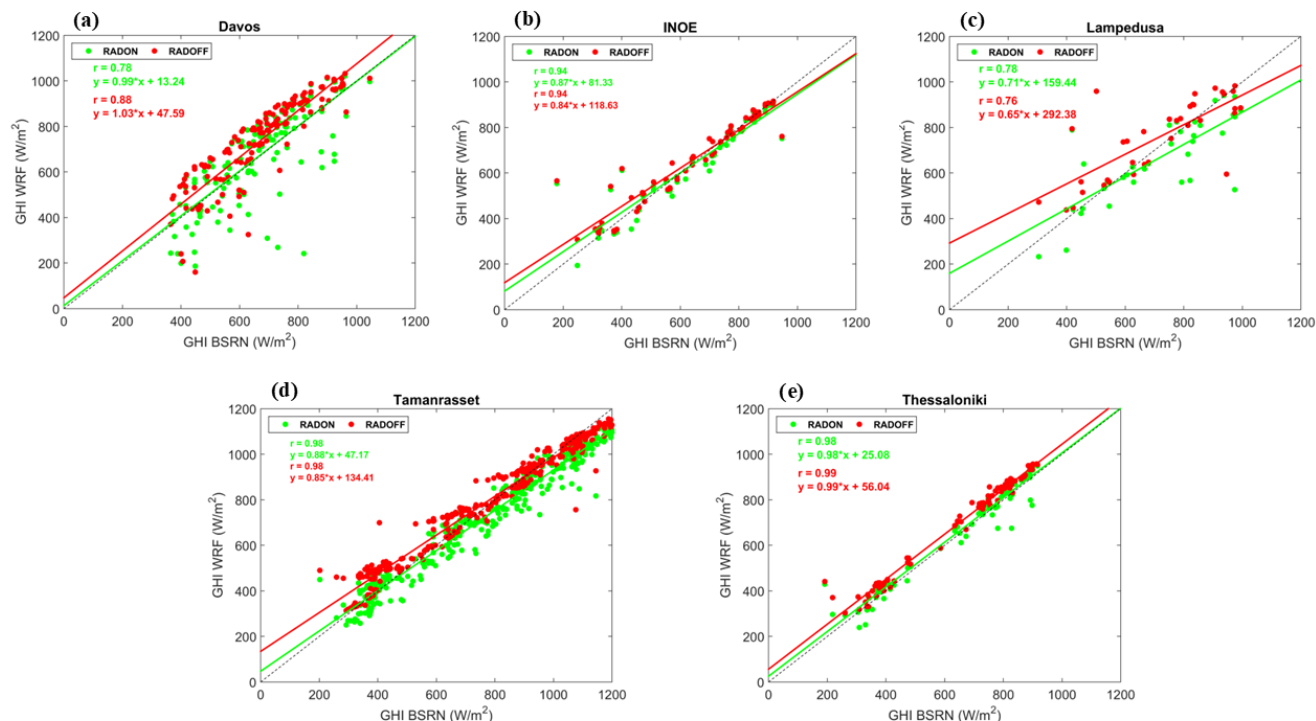
Figure 4 Correlation between the GHI from the pyranometer and the model for RADOFF (red) and RADON (green) for the five sites under clear-sky conditions

320

The average dust optical properties considered in the model are presented in Table 5, while the average measured aerosol optical properties are shown in Table 6. It should be noted that the optical properties in Table 6 are representative of the overall aerosol load over the sites (and not only for dust). By comparing data in Table 5 and Table 6 we conclude that:

- Over INOE the AOD from AERONET is larger than the DOD from the model. Over the other four sites the dust
325   optical depth is generally overestimated by METAL-WRF. The overestimation is similar for RADON and RADOFF with the exception of Tamanrasset where RADON gives more realistic DOD values. Given that during the selected period most of the measured AOD over the stations is due to dust, the differences between the measured and modeled DOD seem to be site dependent.

- The values of SSA, ASY or AE remain practically similar between RADOFF and RADON simulations.

330 - The SSA from the model is in good agreement with the measured SSA for all sites except Davos, where the difference is ~ 0.07. This is possibly because in Davos dust has a relatively smaller contribution in the aerosol mixture relative to the other sites. The SSA from the model and the measurements correspond to slightly different wavelengths (400 nm and 440 nm respectively), which however does not significantly affect the comparison. Comparison for other wavelengths in the range 500 – 1000 nm yielded similar results.

15

335   -   The ASY from the model is in good agreement (within 0.02) with the measured ASY for all sites except Tamanrasset, where the difference is of the order of 0.1. This is possibly because the model cannot capture accurately the bigger dust particles sizes that are abundant at such a short distance from the source. The ASY from the model and the measurements correspond to slightly different wavelengths (400 nm and 440 nm respectively) which again does not affect the comparison significantly. Comparison for other wavelengths in the range 500 – 1000 nm (as for the SSA)

340   yielded similar results.

       -    With the exception of Tamanrasset, the model underestimates the AE values at the measuring stations, which is logical given that the model considers only dust aerosols, while the measurements are also affected by smaller particles from local sources. The larger AE values by the model at Tamanrasset are probably related to the very large particles over the area that are not considered by the model (e.g., Fountoulakis et al., 2024).

345   -   At Davos, the model overestimates the DOD, because the rather coarse spatial grid of 15Km × 15Km cannot properly resolve the impacts of local topography to the atmospheric flow (see Solomos et al., 2018 for more details on orographic impact in dust simulations).

The improved agreement between the measured and modelled GHI for RADON shown in Figure 4, is related to the dust-radiation interactions considered in RADON, which provides simulations closest to reality, with improved radiative transfer

350   in the atmospheric column, improved atmospheric dynamics and ultimately DOD. Changes in water vapor between the two runs have minor effects on the overall difference in simulated GHI.

Table 5 Average dust optical properties that were used by the model to simulate GHI for RADON and RADOFF for the period of study.

355

	mode	Davos	INOE	Lampedusa	Tamanrasset	Thessaloniki
AOD at 500 nm	RADON	0.32 ± 0.41	0.09 ± 0.18	0.42 ± 0.53	0.36 ± 0.27	0.18 ± 0.26
	RADOFF	0.35 ± 0.50	0.11 ± 0.21	0.44 ± 0.55	0.45 ± 0.41	0.21 ± 0.30
SSA at 400 nm	RADON	0.91 ± 0.01	0.91 ± 0.01	0.90 ± 0.01	0.90 ± 0.01	0.91 ± 0.01
	RADOFF	0.91 ± 0.01	0.91 ± 0.01	0.90 ± 0.01	0.90 ± 0.01	0.90 ± 0.01
ASY at 400 nm	RADON	0.71 ± 0.01	0.71 ± 0.01	0.71 ± 0.01	0.71 ± 0.01	0.71 ± 0.01
	RADOFF	0.71 ± 0.01	0.71 ± 0.01	0.71 ± 0.01	0.71 ± 0.01	0.71 ± 0.01
AE (400–600 nm)	RADON	0.29 ± 0.20	0.18 ± 0.22	0.31 ± 0.21	0.39 ± 0.13	0.26 ± 0.20
	RADOFF	0.31 ± 0.18	0.18 ± 0.21	0.28 ± 0.20	0.39 ± 0.12	0.27 ± 0.20

360

Table 6 Average aerosol optical properties that from AERONET that correspond to RADON and RADOFF for the period of study.

	mode	Davos	INOE	Lampedusa	Tamanrasset	Thessaloniki
AOD at 500 nm	RADON	0.07 ± 0.04	0.18 ± 0.14	0.42 ± 0.35	0.26 ± 0.20	0.18 ± 0.09
	RADOFF	0.07 ± 0.04	0.18 ± 0.14	0.42 ± 0.36	0.26 ± 0.20	0.18 ± 0.09
SSA at 440 nm	RADON	0.84 ± 0.08	0.93 ± 0.01	0.91 ± 0.02	0.90 ± 0.02	0.92 ± 0.05
	RADOFF	0.84 ± 0.09	0.93 ± 0.01	0.91 ± 0.02	0.90 ± 0.02	0.92 ± 0.05
ASY at 440 nm	RADON	0.72 ± 0.04	0.69 ± 0.03	0.70 ± 0.04	0.82 ± 0.02	0.69 ± 0.04
	RADOFF	0.72 ± 0.05	0.69 ± 0.03	0.70 ± 0.04	0.82 ± 0.02	0.69 ± 0.04
AE (440 – 675 nm)	RADON	1.39 ± 0.26	1.24 ± 0.05	0.69 ± 0.52	0.14 ± 0.08	1.11 ± 0.50
	RADOFF	1.39 ± 0.26	1.26 ± 0.05	0.69 ± 0.52	0.14 ± 0.08	1.11 ± 0.50

3.1.2. All-sky

365 The comparison between the measured and modelled GHI, for cases when METAL-WRF simulates DOD (at 500 nm) that is larger than 0.05 is shown in Figure 5. In Figure 6 the same comparison is performed for the cases when DOD<0.05 (i.e., when the contribution of dust is not very significant). In general, METAL-WRF overestimates GHI under cloudy conditions, but the comparison is improved for RADON when a significant amount of dust is present (Figure 5). This improvement is larger compared to the improvement for the clear-sky cases, which is due to the more accurate representation of cloud properties in

370 the RADON runs (see Figure 7 as an example). For small dust amounts, switching from RADOFF to RADON does not have any significant impact on the GHI (Figure 6). Comparing the two figures (Figure 5 and Figure 6) further confirms that the main improvement between the two sensitivity runs, is the improved representation of the impact of dust on radiative transfer processes, either directly through dust-radiation interactions, or semi-directly through the improved representation of clouds. Since the dust particles are not considered as CCN or IN in any of our simulations, the more accurate description of cloudiness

375 in the model is attributed to the more accurate calculation of heating rates and energy flux distribution along the atmospheric column (semi-direct effect; Spyrou et al., 2010; 2013). The correlation between the precipitable water atmospheric content (i.e., the amount of water vapor in the atmosphere) from measurements and the model is shown indicatively in Figure 8 for Lampedusa. Differences in water vapor content for the two modes (RADON/RADOFF) were in all cases found to be small and are estimated to have a much smaller impact compared to the differences in the DOD, as expected for stations away from

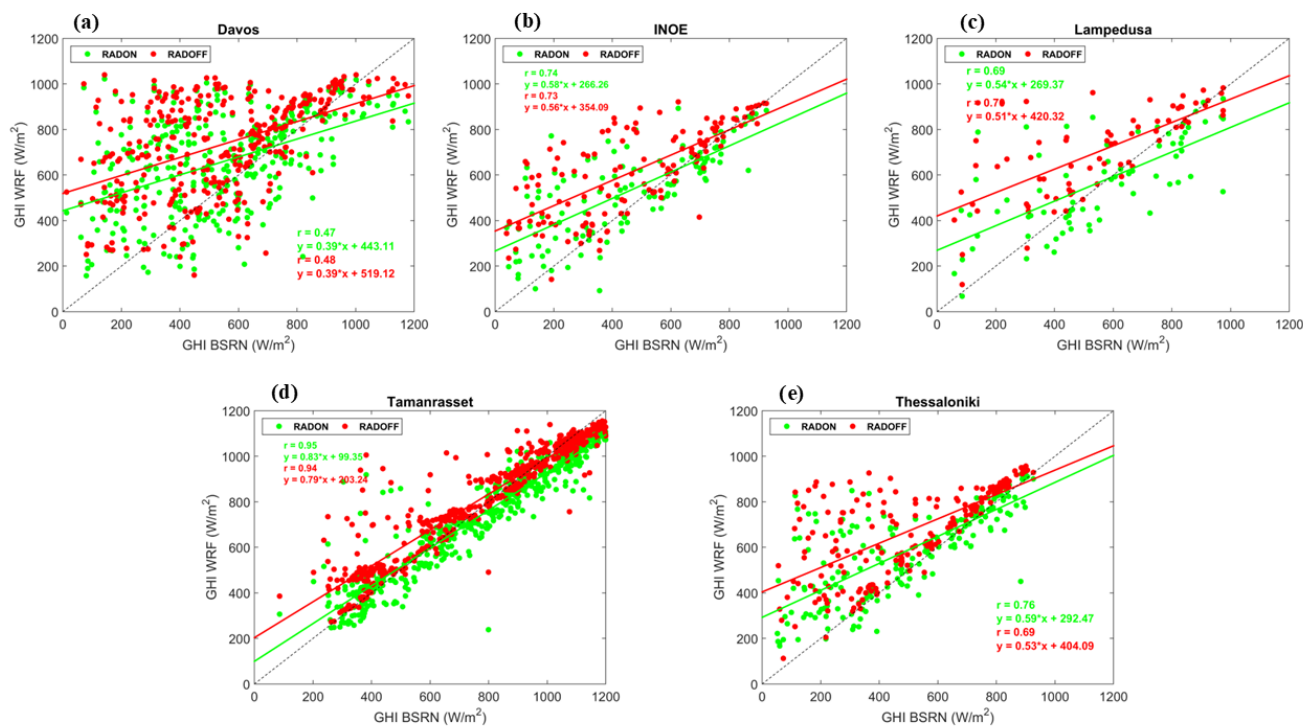380 the dust sources (Spyrou 2018).

Figure 5 Correlation between the GHI from the pyranometer and the model for RADOFF (red) and RADON (green) for the five sites under all sky conditions for DOD>0.05.
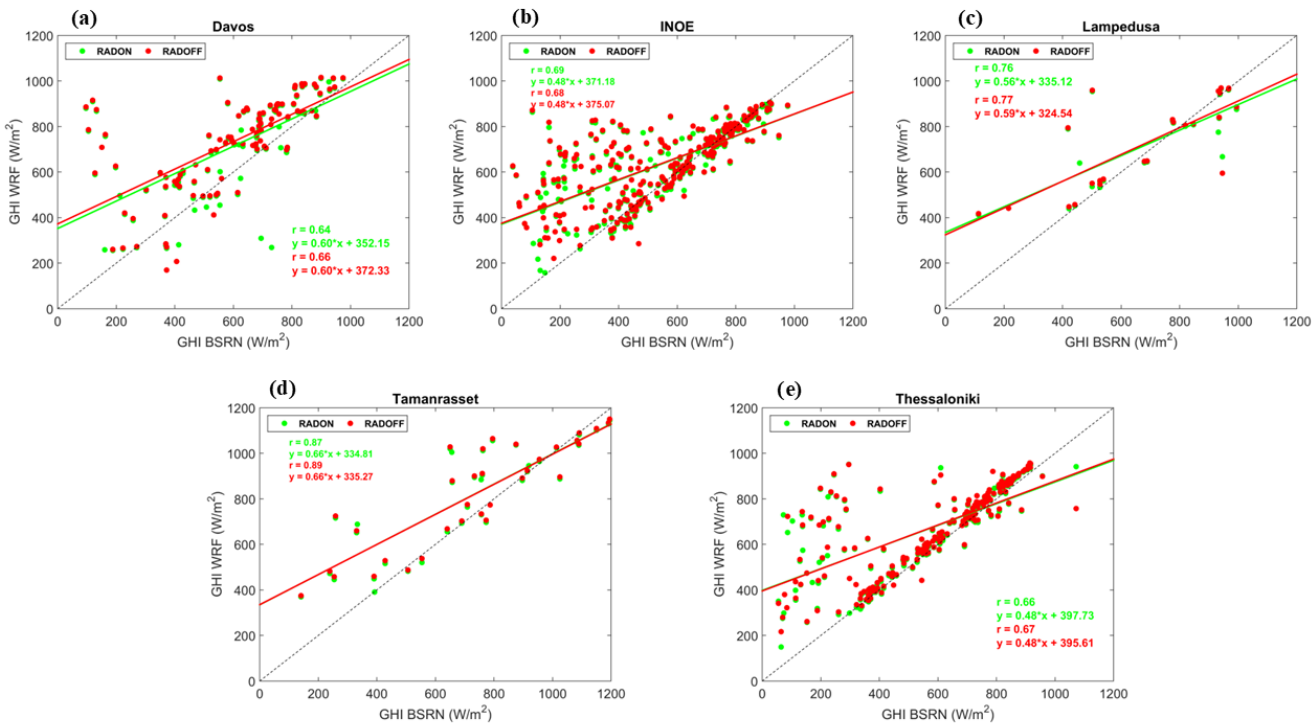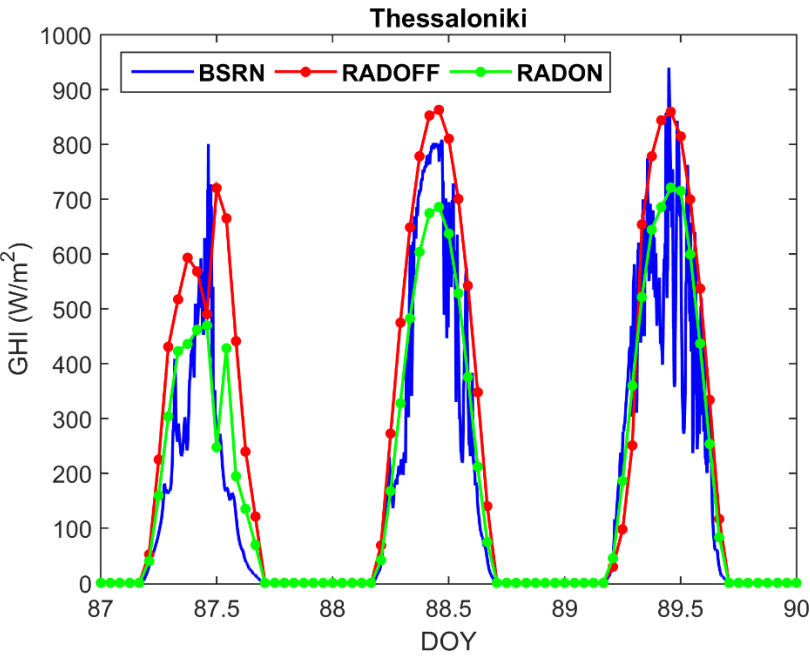
Figure 6 Correlation between the GHI from the pyranometer and the model for RADOFF (red) and RADON (green) for the five sites under all sky conditions for DOD<0.05.

Figure 7 GHI from BSRN and the model for cloudy days in Thessaloniki.
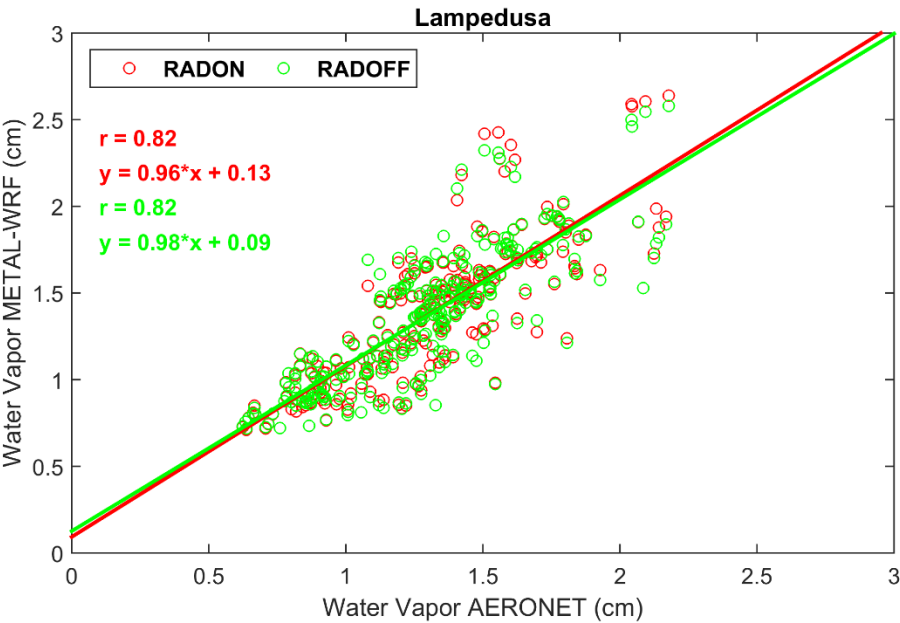

Figure 8 Correlation between the precipitable water content from AERONET and the METAL-WRF for RADON and RADOFF.

20

4 Conclusions

In this study we present the implementation of radiative transfer calculations for each mineral-dust type, in METAL-WRF model. The first step was to update the RRTMG radiative transfer scheme of the model by including the optical properties of the prognostic minerals. The optical properties were based on previous measuring studies and are the state-of-the-art of existing data for the entire radiative spectrum needed by the RT algorithm. After the successful implementation of the new radiative transfer scheme, two sets of simulations were performed, in order to examine the validity of the methodology and quantify the potential benefits from the process: The RADON set of simulations, where mineral radiative impacts are included in the calculations and the RADOFF, where dust and minerals are considered as passive tracers. A two-month simulation period was selected, namely March and April 2022, which was a very active period, with a series of dust/mineral transport events from the Saharan desert, over the Mediterranean and towards Europe.

The simulation results were compared against ground-based GHI data and AERONET optical properties that were measured at five sites, namely Tamanrasset in Algeria, Thessaloniki in Greece, Magurele (INOE) in Romania, Davos in Switzerland and Lampedusa in Italy. At all five sites, the GHI is overestimated when the dust-radiation interactions are not considered. An improvement (values are closer to the y=x line) was observed in all sites for RADON runs, especially for Tamanrasset, due to its proximity to the source areas, since the improvement is larger over sites where aerosol mixture is dominated by dust aerosols. Though, even at sites where many species contribute to the aerosol mixture, the improvement in the agreement between the model and the measurements is clear.

In general, METAL-WRF overestimates GHI under cloudy conditions, which makes the simulations more uncertain when the stations are strongly affected by clouds. Although a small improvement is evident for RADON compared to RADOFF, the overestimation of the GHI under cloudy conditions remains large. The most problematic site is Davos, where the relatively coarse model resolution used in the current study makes it difficult to accurately represent the orographic variability and the resulting implications on local atmospheric circulation and phenomena. The use of finer resolution nested grids could probably improve the model performance at this station.

For the dust optical depth, the RADON simulations still provide more realistic values in all simulations of METAL-WRF. The largest overestimation was found over the mountainous site of Davos (~ 0.25), and was less significant over lower altitude sites. This discrepancy can be attributed to the resolution issues discussed above. Changing from radiative passive (RADOFF) to radiative active minerals does not practically change single scattering albedo, asymmetry parameter or Angstrom exponent. This work is the first step towards the direction of more accurate radiative transfer calculations, by considering the separate optical properties of the different minerals in the atmospheric mixture. Further improvements that will be built upon the current version of METAL-WRF include more detailed aerosol sources and satellite derived dust mineralogy (e.g. from EMIT mission) as well as more detailed measured optical properties of all the mineral components of desert dust. The model developments and sensitivity tests that are shown in this work present the improved capabilities of METAL-WRF to simulate the chemical composition of dust particles in the atmosphere along with their contribution to radiative transfer processes. The new

developments improve the capability of the model to describe the air-quality and meteorological conditions and also to provide detailed forecasts for solar energy applications, especially at areas that are often affected by dust intrusions such as the North

430 Africa and the Mediterranean.

440 **References**

- Ackerman, T. P. and Toon, O. B.: Absorption of visible radiation in atmosphere containing mixtures of absorbing and non-absorbing particles, Appl. Optics, 20(20), 3661–3662, 1981.

- Adeyemi A. Adebiyi, Jasper F. Kok, 2020. Climate models miss most of the coarse dust in the atmosphere. Sci. Adv.6,eaaz9507(2020).DOI:10.1126/sciadv.aaz9507

445 - Ageitos, Gonçalves M., Obiso, V., Miller, R. L., Jorba, O., Klose, M., Dawson, M., Balkanski, Y., Perlwitz, J., Basart, S., Di Tomaso, E., Escribano, J., Macchia, F., Montané, G., Mahowald, N. M., Green, R. O., Thompson, D. R., and Pérez García-Pando, C.: Modeling dust mineralogical composition: sensitivity to soil mineralogy atlases and their expected climate impacts, Atmos. Chem. Phys., 23, 8623–8657, https://doi.org/10.5194/acp-23-8623-2023, 2023.

- Barnard, J. C., Fast, J. D., Paredes-Miranda, G., Arnott, W. P., and Laskin, A.: Technical Note: Evaluation of the WRF-
450 Chem "Aerosol Chemical to Aerosol Optical Properties" Module using data from the MILAGRO campaign, Atmos. Chem. Phys., 10, 7325–7340, https://doi.org/10.5194/acp-10-7325-2010, 2010.

- Bergas-Massó, E., Gonçalves Ageitos, M., Myriokefalitakis, S., Miller, R. L., van Noije, T., Le Sager, P., et al. (2023). Pre-industrial, present and future atmospheric soluble iron deposition and the role of aerosol acidity and oxalate under CMIP6 emissions. Earth's Future, 11, e2022EF003353. https://doi.org/10.1029/2022EF003353.

455 - Bond, T. C., G. Habib, and R. W. Bergstrom (2006), Limitations in the enhancement of visible light absorption due to mixing state, J. Geophys. Res., 111, D20211, doi:10.1029/2006JD007315.

- Chen, S., Huang, J., Kang, L., Wang, H., Ma, X., He, Y., Yuan, T., Yang, B., Huang, Z., and Zhang, G.: Emission, transport, and radiative effects of mineral dust from the Taklimakan and Gobi deserts: comparison of measurements and model results, Atmos. Chem. Phys., 17, 2401–2421, https://doi.org/10.5194/acp-17-2401-2017, 2017.

460 • Cheng, T., Chen, H., Gu, X., Yu, T., Guo, J., & Guo, H. (2012). The inter-comparison of MODIS, MISR and GOCART aerosol products against AERONET data over China. Journal of Quantitative Spectroscopy and Radiative Transfer, 113(16), 2135–2145. https://doi.org/10.1016/j.jqsrt.2012.06.016.

• Claquin, T., Schulz, M., and Balkanski, Y.: Modeling the mineralogy of atmospheric dust sources, 1999. J. Geophys. Res., 104, p.22243-22256. doi: 10.1029/1999JD900416 hal-02870447

465 • Claquin, T.; Schulz, M.; Balkanski, Y. Modeling the mineralogy of atmospheric dust sources. J. Geophys. Res. 1999, 104, 22243–22256. https://doi.org/10.1029/1999JD900416.

• Creamean, J. M., Suski, K. J., Rosenfeld, D., Cazorla, A., DeMott, P. J., Sullivan, R. C., White, A. B., Ralph, F. M., Minnis, P., Comstock, J. M., Tomlinson, J. M., and Prather, K. A.: Dust and Biological Aerosols from the Sahara and Asia Influence Precipitation in the Western U.S., Science, 339, 1572–1578, https://doi.org/10.1126/science.1227279, 470 2013.

• Derimian, Y., A. Karnieli, Y. J. Kaufman, M. O. Andreae, T. W. Andreae, O. Dubovik, W. Maenhaut, I. Koren, and B. N. Holben (2006), Dust and pollution aerosols over the Negev desert, Israel: Properties, transport, and radiative effect, J. Geophys. Res., 111, D05205, doi:10.1029/2005JD006549.

• Driemel, A., Augustine, J., Behrens, K., Colle, S., Cox, C., Cuevas-Agulló, E., Denn, F. M., Duprat, T., Fukuda, M., 475 Grobe, H., Haeffelin, M., Hodges, G., Hyett, N., Ijima, O., Kallis, A., Knap, W., Kustov, V., Long, C. N., Longenecker, D., Lupi, A., Maturilli, M., Mimouni, M., Ntsangwane, L., Ogihara, H., Olano, X., Olefs, M., Omori, M., Passamani, L., Pereira, E. B., Schmithüsen, H., Schumacher, S., Sieger, R., Tamlyn, J., Vogt, R., Vuilleumier, L., Xia, X., Ohmura, A., and König-Langlo, G.: Baseline Surface Radiation Network (BSRN): structure and data description (1992–2017), Earth Syst. Sci. Data, 10, 1491–1501, https://doi.org/10.5194/essd-10-1491-2018, 2018.

480 • Dubovik, O. and M. D. King, "A flexible inversion algorithm for retrieval of aerosol optical properties from Sun and sky radiance measurements", J. Geophys. Res., 105, 20,673-20,696, 2000. https://doi.org/10.1029/2000JD900282

• Egan, Walter G. and Theodore W. Hilgeman, 1979. Optical Properties of Inhomogeneous Materials Applications to Geology, Astronomy, Chemistry and Engineering. ISBN-13: 978-0-12-232650-9, ISBN: 0-12-232650-4

• Esmaeil N., M. Gharagozloo, A. Rezaei, G. Grunig 2014: Dust events, pulmonary diseases and immune system, Am J 485 Clin Exp Immunol 2014 3(1):20-29, 2014.

• Fan, R., Ma, Y., Jin, S., Gong, W., Liu, B., Wang, W., Li, H. and Zhang, Y., 2023. Validation, analysis, and comparison of MISR V23 aerosol optical depth products with MODIS and AERONET observations. Science of the Total Environment, 856, p.159117. https://doi.org/10.1016/j.scitotenv.2022.159117

• Fast, J. D., W. I. Gustafson Jr., R. C. Easter, R. A. Zaveri, J. C. Barnard, E. G. Chapman, G. A. Grell, and S. E. Peckham 490 (2006), Evolution of ozone, particulates, and aerosol direct radiative forcing in the vicinity of Houston using a fully coupled meteorology-chemistry-aerosol model, J. Geophys. Res., 111, D21305, doi:10.1029/2005JD006721.

- Fountoulakis, I., Tsekeri, A., Kazadzis, S., Amiridis, V., Nersesian, A., Tsichla, M., Proestakis, E., Gkikas, A., Papachristopoulou, K., Barlakas, V., Emde, C., and Mayer, B.: A sensitivity study on radiative effects due to the parameterization of dust optical properties in models, Atmos. Chem. Phys., 24, 4915–4948, https://doi.org/10.5194/acp-24-4915-2024, 2024.

- Fountoulakis, I.; Kosmopoulos, P.; Papachristopoulou, K.; Raptis, I.-P.; Mamouri, R.-E.; Nisantzi, A.; Gkikas, A.; Witthuhn, J.; Bley, S.; Moustaka, A.; et al. Effects of Aerosols and Clouds on the Levels of Surface Solar Radiation and Solar Energy in Cyprus. Remote Sens. 2021, 13, 2319. https://doi.org/10.3390/rs13122319

- G. Varlas, V. Vervatis, C. Spyrou, E. Papadopoulou, A. Papadopoulos, P. Katsafados, (2020) Investigating the impact of atmosphere–wave–ocean interactions on a Mediterranean tropical-like cyclone, Ocean Modelling, Volume 153, 2020, 101675, ISSN 1463-5003, doi: 10.1016/j.ocemod.2020.101675.

- Giles, D. M., Sinyuk, A., Sorokin, M. G., Schafer, J. S., Smirnov, A., Slutsker, I., Eck, T. F., Holben, B. N., Lewis, J. R., Campbell, J. R., Welton, E. J., Korkin, S. V., and Lyapustin, A. I.: Advancements in the Aerosol Robotic Network (AERONET) Version 3 database – automated near-real-time quality control algorithm with improved cloud screening for Sun photometer aerosol optical depth (AOD) measurements, Atmos. Meas. Tech., 12, 169–209, https://doi.org/10.5194/amt-12-169-2019, 2019.

- Ginoux, P., Chin, M., Tegen, I., Goddard, T., and In, G.: Sources and distributions of dust aerosols simulated with the GOCART model, J. Geophys. Res., 106, 20255–20273, 2001.

- Ginoux, P., Chin, M., Tegen, I., Goddard, T., and In, G.: Sources and distributions of dust aerosols simulated with the GOCART model, J. Geophys. Res., 106, 20255–20273, 2001.

- Gkikas, A., Obiso, V., Pérez García-Pando, C., Jorba, O., Hatzianastassiou, N., Vendrell, L., Basart, S., Solomos, S., Gassó, S., and Baldasano, J. M.: Direct radiative effects during intense Mediterranean desert dust outbreaks, Atmos. Chem. Phys., 18, 8757–8787, https://doi.org/10.5194/acp-18-8757-2018, 2018.

- GLORYS12V1 product. E.U. Copernicus Marine Service Information (CMEMS). Marine Data Store (MDS). DOI (product): https://doi.org/10.48670/moi-00021.

- Grell, G. A. and Freitas, S. R., 2014: A scale and aerosol aware stochastic convective parameterization for weather and air quality modeling, Atmos. Chem. Phys., 14, 5233-5250, doi:10.5194/acp-14-5233-2014.

- Grell, G. A., Peckham, S. E., Schmitz, R., McKeen, S. A., Frost, G., Skamarock, W. C., and Eder, B. (2005): Fully coupled "online" chemistry within the WRF model, Atmos. Environ., 39, 6957–6975.

- Hamilton, D. S., Scanza, R. A., Feng, Y., Guinness, J., Kok, J. F., Li, L., Liu, X., Rathod, S. D., Wan, J. S., Wu, M., and Mahowald, N. M.: Improved methodologies for Earth system modelling of atmospheric soluble iron and observation comparisons using the Mechanism of Intermediate complexity for Modelling Iron (MIMI v1.0), Geosci. Model Dev., 12, 3835–3862, https://doi.org/10.5194/gmd-12-3835-2019, 2019.

- Hersbach, H.; Bell, B.; Berrisford, P.; Hirahara, S.; Horányi, A.; Muñoz-Sabater, J.; Nicolas, J.; Peubey, C.; Radu, R.;
525   Schepers, D.; et al. The ERA5 global reanalysis. Q. J. R. Meteorol. Soc. 2020, 146, 1999–2049.

- Holben, B. N., Eck, T. F., Slutsker, I., Tanré, D., Buis, J. P., Setzer, A., Vermote, E., Reagan, J. A., Kaufman, Y. J., Nakajima, T., Lavenu, F., Jankowiak, I., and Smirnov, A.: AERONET – A federated instrument network and data archive for aerosol characterization, Remote Sens. Environ., 66, 1–16, https://doi.org/10.1016/S0034-4257(98)00031-5, 1998.

- Holben, B.N., D. Tanre, A. Smirnov, T.F. Eck, I. Slutsker, N. Abuhassan, W.W. Newcomb, J.S. Schafer, B. Chatenet, F.
530   Lavenu, Y.J. Kaufman, Vande Castle, J. Setzer, A. Markham, B. Clark, D. Frouin, R. Halthore, R. Karneli, A. O'Neill, N.T. Pietras, C. Pinker, R.T. Voss, K. Zibordi, G. An emerging ground-based aerosol climatology: aerosol optical depth from AERONET, J. Geophys. Res., 106 (2001), pp. 12067-12097, 10.1029/2001JD900014

- Iacono, M. J., J. S. Delamere, E. J. Mlawer, M. W. Shephard, S. A. Clough, and W. D. Collins, 2008: Radiative forcing by long–lived greenhouse gases: Calculations with the AER radiative transfer models. J. Geophys. Res., 113, D13103.
535   doi:10.1029/2008JD009944

- Ito, T., Nenes, A., Johnson, M. S., Meskhidze, N., Valett, J., and Deutsch, C. (2016) Late 20th century deoxygenation of the tropical Pacific enhanced by aerosol pollutants, Nature Geosci., doi:10.1038/ngeo2717.

- Janjic, Z. I., 1996: The surface layer in the NCEP Eta Model. Eleventh conference on numerical weather prediction, Norfolk, VA, 19–23 August 1996. Amer Meteor Soc, Boston, MA, pp 354–355.

540 - Janjic, Z. I., 2002: Nonsingular implementation of the Mellor-Yamada Level 2.5 Scheme in the NCEP Meso model. NCEP Office Note No. 437, 61 pp.

- Janjic, Zavisa I., 1994: The Step–Mountain Eta Coordinate Model: Further developments of the convection, viscous sublayer, and turbulence closure schemes. Mon. Wea. Rev., 122, 927–945. doi:10.1175/1520-0493(1994)122%3c0927:TSMECM%3e2.0.CO;2

545 - Kallos, G.; S. Solomos; J. Kushta; C. Mitsakou; C. Spyrou; N. Bartsotas; C. Kalogeri, 2014: Natural and anthropogenic aerosols in the Eastern Mediterranean and Middle East: Possible impacts, Science of the Total Environment, 488–489 (2014) 389–397, doi: 10.1016/j.scitotenv.2014.02.035.

- Kaskaoutis, D. G., K. V. S. Badarinath, S. Kumar Kharol, A. Rani Sharma, and H. D. Kambezidis (2009), Variations in the aerosol optical properties and types over the tropical urban site of Hyderabad, India, J. Geophys. Res., 114, D22204,
550   doi:10.1029/2009JD012423.

- Kok, J.; Storelvmo, T.; Karydis, V.; Adebiyi, A.; Mahowald, N.; & Evan, A.; & He, C.; & Leung, D. (2023). Mineral dust aerosol impacts on global climate and climate change. Nature Reviews Earth & Environment. 4. 10.1038/s43017-022-00379-5.

- Kosmopoulos, P.G.; Kazadzis, S.; El-Askary, H.; Taylor, M.; Gkikas, A.; Proestakis, E.; Kontoes, C.; El-Khayat, M.M.
555   Earth-Observation-Based Estimation and Forecasting of Particulate Matter Impact on Solar Energy in Egypt. Remote Sens. 2018, 10, 1870. https://doi.org/10.3390/rs10121870

- LeGrand, S. L., Polashenski, C., Letcher, T. W., Creighton, G. A., Peckham, S. E., and Cetola, J. D.: The AFWA dust emission scheme for the GOCART aerosol model in WRF-Chem v3.8.1, Geosci. Model Dev., 12, 131–166, https://doi.org/10.5194/gmd-12-131-2019, 2019.

560
- LeGrand, S. L., Polashenski, C., Letcher, T. W., Creighton, G. A., Peckham, S. E., and Cetola, J. D.: The AFWA dust emission scheme for the GOCART aerosol model in WRF-Chem v3.8.1, Geosci. Model Dev., 12, 131–166, https://doi.org/10.5194/gmd-12-131-2019, 2019.

- Levin, Z. and W.R. Cotton, Aerosol Pollution Impact on Precipitation: A Scientific Review. WMO/IUGG International Aerosol Precipitation Science Assessment Group (IAPSAG). pp 485, 2007.

565
- Li, L., Mahowald, N. M., Miller, R. L., Pérez García-Pando, C., Klose, M., Hamilton, D. S., Gonçalves Ageitos, M., Ginoux, P., Balkanski, Y., Green, R. O., Kalashnikova, O., Kok, J. F., Obiso, V., Paynter, D., and Thompson, D. R.: Quantifying the range of the dust direct radiative effect due to source mineralogy uncertainty, Atmos. Chem. Phys., 21, 3973–4005, https://doi.org/10.5194/acp-21-3973-2021, 2021.

- Li, L., Mahowald, N. M., Miller, R. L., Pérez García-Pando, C., Klose, M., Hamilton, D. S., Gonçalves Ageitos, M.,
570 Ginoux, P., Balkanski, Y., Green, R. O., Kalashnikova, O., Kok, J. F., Obiso, V., Paynter, D., and Thompson, D. R.: Quantifying the range of the dust direct radiative effect due to source mineralogy uncertainty, Atmos. Chem. Phys., 21, 3973–4005, https://doi.org/10.5194/acp-21-3973-2021, 2021.

- Li, L., Mahowald, N. M., Miller, R. L., Pérez García-Pando, C., Klose, M., Hamilton, D. S., Gonçalves Ageitos, M., Ginoux, P., Balkanski, Y., Green, R. O., Kalashnikova, O., Kok, J. F., Obiso, V., Paynter, D., and Thompson, D. R.:
575 Quantifying the range of the dust direct radiative effect due to source mineralogy uncertainty, Atmos. Chem. Phys., 21, 3973–4005, https://doi.org/10.5194/acp-21-3973-2021, 2021.

- Liu, Y., Jia, R., Dai, T., Xie, Y., and Shi, G. (2014). A review of aerosol optical properties and radiative effects. J. Meteor. Res., 28:1003–1028. doi:10.1007/s13351-014-4045-z.

- Long, L.L., M.R. Querry, R.J. Bell, R.W. Alexander, Optical properties of calcite and gypsum in crystalline and powdered
580 form in the infrared and far-infrared, Infrared Physics, Volume 34, Issue 2, 1993, Pages 191-201, ISSN 0020-0891, https://doi.org/10.1016/0020-0891(93)90008-U.

- Meloni D., A. di Sarra, G. Biavati.,J.J. DeLuisi, F. Monteleone, G. Pace, S. Piacentino, D.M. Sferlazzo (2007), Seasonal behavior of Saharan dust events at the Mediterranean island of Lampedusa in the period 1999-2005, Atmos. Environ., 41, 3041-3056, 10.1016/j.atmosenv.2006.12.001.

585
- Mesinger, F., 1993: Forecasting upper tropospheric turbulence within the framework of the Mellor-Yamada 2.5 closure. Res. Activ. in Atmos. and Ocean. Mod., WMO, Geneva, CAS/JSC WGNE Rep. No. 18, 4.28-4.29.

- Miller, B. B. and Carter, C.: The test article, J. Sci. Res., 12, 135–147, doi:10.1234/56789, 2015.

- Mishra S. K., Dey Sagnik and S. N. Tripathi 2008: Implications of particle composition and shape to dust radiative effect: A case study from the Great Indian Desert. Geophysical Research Letters ,35,L23814,doi:10.1029/2008GL036058.

590   • Mitsakou, C., Kallos, G., Papantoniou, N., Spyrou, C., Solomos, S., Astitha, M., and Housiadas, C.: Saharan dust levels in Greece and received inhalation doses, Atmos. Chem. Phys., 8, 7181-7192, 2008

• Mlawer, Eli. J., Steven. J. Taubman, Patrick. D. Brown, M. J. Iacono, and S. A. Clough,1997: Radiative transfer for inhomogeneous atmospheres: RRTM, a validated correlated–k model for the longwave. J. Geophys. Res., 102, 16663–16682. doi:10.1029/97JD00237

595   • Natsis, A.; Bais, A.; Meleti, C. Trends from 30-Year Observations of Downward Solar Irradiance in Thessaloniki, Greece. Appl. Sci. 2024, 14, 252. https://doi.org/10.3390/app14010252. https://doi.org/10.1016/j.solener.2018.03.044

• Nickovic, S., Vukovic, A., Vujadinovic, M., Djurdjevic, V., and Pejanovic, G.: Technical Note: High-resolution mineralogical database of dust-productive soils for atmospheric dust modeling, Atmos. Chem. Phys., 12, 845-855, doi:10.5194/acp-12-845-2012, 2012.

600   • Nickovic, S.; Vukovic, A.; Vujadinovic, M.; Djurdjevic, V.; Pejanovic, G. Technical Note: High-resolution mineralogical database of dust-productive soils for atmospheric dust modeling. Atmos. Chem. Phys. 2012, 12, 845–855. https://doi.org/10.5194/acp-12-845-2012.

• O'Neill, N. T., Eck, T. F., Smirnov, A., Holben, B. N., & Thulasiraman, S. (2003). Spectral discrimination of coarse and fine mode optical depth. Journal of Geophysical Research: Atmospheres, 108, 4559–4573.
605   https://doi.org/10.1029/2002JD002975.

• Obiso, V., Gonçalves Ageitos, M., Miller, R. L., Pérez García-Pando, C., Schuster, G. L., Bauer, S. E., Di Biagio, C., Formenti, P., Jorba, O., Perlwitz, J. P., and Tsigaridis, K.: Regional variations in dust shortwave absorption explained predominantly by mineralogical composition, in preparation, 2023

• Papachristopoulou, K.; Fountoulakis, I.; Gkikas, A.; Kosmopoulos, P.G.; Nastos, P.T.; Hatzaki, M.; Kazadzis, S. 15-Year
610   Analysis of Direct Effects of Total and Dust Aerosols in Solar Radiation/Energy over the Mediterranean Basin. Remote Sens. 2022, 14, 1535. https://doi.org/10.3390/rs14071535

• Perlwitz, J. P., Pérez García-Pando, C., and Miller, R. L.: Predicting the mineral composition of dust aerosols – Part 1: Representing key processes, Atmos. Chem. Phys., 15, 11593–11627, https://doi.org/10.5194/acp-15-11593-2015, 2015

• Prospero, J.M.; Ginoux, P.; Torres, O.; Nicholson, S.E.; Gill, T.E. Environmental Characterization of Global Sources of
615   Atmospheric Soil Dust Identified with the Nimbus 7 Total Ozone Mapping Spectrometer (Toms) Absorbing Aerosol Product. Rev. Geophys. 2002, 40, 1002.

• Querry M., Optical Constants of Minerals and Other Materials from the Millimeter to the Ultraviolet Report CRDEC-CR-88009, US Army, Aberdeen, 1987

• Rap, A., Scott, C. E., Spracklen, D. V., Bellouin, N., Forster, P. M., Carslaw, K. S., Schmidt, A., and Mann, G. (2013).
620   Natural Aerosol Direct and Indirect Radiative Effects. Geophys. Res. Lett., 40:3297–3301. doi:10.1002/grl.50441.

- Rodriguez-Navarro, C., di Lorenzo, F., and Elert, K.: Mineralogy and physicochemical features of Saharan dust wet deposited in the Iberian Peninsula during an extreme red rain event, Atmos. Chem. Phys., 18, 10089–10122, https://doi.org/10.5194/acp-18-10089-2018, 2018.

625
- Rothman, L.S., C.P. Rinsland, A. Goldman, S.T. Massie, D.P. Edwards, J-M. Flaud, A. Perrin, C. Camy-Peyret, V. Dana, J.-Y. Mandin, J. Schroeder, A. Mccann, R.R. Gamache, R.B. Wattson, K. Yoshino, K.V. Chance, K.W. Jucks, L.R. Brown, V. Nemtchinov, P. Varanasi. THE HITRAN MOLECULAR SPECTROSCOPIC DATABASE AND HAWKS (HITRAN ATMOSPHERIC WORKSTATION): 1996 EDITION, Journal of Quantitative Spectroscopy and Radiative Transfer, Volume 60, Issue 5, Pages 665-710, 1998, ISSN 0022-4073,https://doi.org/10.1016/S0022-4073(98)00078-8.

- Scanza, R. A., Mahowald, N., Ghan, S., Zender, C. S., Kok, J. F., Liu, X., Zhang, Y., and Albani, S.: Modeling dust as
630 component minerals in the Community Atmosphere Model: development of framework and impact on radiative forcing, Atmos. Chem. Phys., 15, 537–561, https://doi.org/10.5194/acp-15-537-2015, 2015.

- Scanza, R. A., Mahowald, N., Ghan, S., Zender, C. S., Kok, J. F., Liu, X., Zhang, Y., and Albani, S.: Modeling dust as component minerals in the Community Atmosphere Model: development of framework and impact on radiative forcing, Atmos. Chem. Phys., 15, 537–561, https://doi.org/10.5194/acp-15-537-2015, 2015.

635
- Schepanski, Kerstin & Knippertz, Peter & Fiedler, Stephanie & Timouk, Franck & Demarty, J. (2014). The sensitivity of nocturnal low-level jets and near-surface winds over the Sahel to model resolution, initial conditions and boundary-layer setup. Quarterly Journal of the Royal Meteorological Society. 141. 10.1002/qj.2453.

- Sinyuk, A., Holben, B. N., Eck, T. F., Giles, D. M., Slutsker, I., Korkin, S., Schafer, J. S., Smirnov, A., Sorokin, M., and Lyapustin, A.: The AERONET Version 3 aerosol retrieval algorithm, associated uncertainties and comparisons to Version
640 2, Atmos. Meas. Tech., 13, 3375–3411, https://doi.org/10.5194/amt-13-3375-2020, 2020.

- Skamarock, W. C., Klemp, J. B., Dudhia, J., Gill, D. O., Liu, Z., Berner, J., … Huang, X. -yu. (2021). A Description of the Advanced Research WRF Model Version 4.3 (No. NCAR/TN-556+STR). doi:10.5065/1dfh-6p97

- Smith, A. A., Carter, C., and Miller, B. B.: More test articles, J. Adv. Res., 35, 13–28, doi:10.2345/67890, 2014.

- Sokolik, I. N. and Toon, O. B.: Direct radiative forcing by anthropogenic airborne mineral aerosols, Nature, 381, 681–
645 683, 1996.

- Sokolik, I. N. and Toon, O. B.: Incorporation of mineralogical composition into models of the radiative properties of mineral aerosol form UV to IR wavelengths, J. Geophys. Res., 104, 9423–9444, 1999.

- Solomos, S., Kallos, G., Mavromatidis, E., and Kushta, J.: Density currents as a desert dust mobilization mechanism, Atmos. Chem. Phys., 12, 11199–11211, https://doi.org/10.5194/acp-12-11199-2012, 2012.

650
- Solomos, S., S. Nickovic, V. Amiridis, G. Pejanovic, Y. Pradhan, F. Marenco, S. Petkovic, E. Marinou, B. Cvetkovic and C. Kontoes, Development of a Dust Assimilation System for NMM-DREAM from MSG-SEVIRI, Persp. Atmospheric Sciences, doi:10.1007/978-3-319-35095-0_115, 2017

- Solomos, S.; Kalivitis, N.; Mihalopoulos, N.; Amiridis, V.; Kouvarakis, G.; Gkikas, A.; Binietoglou, I.; Tsekeri, A.; Kazadzis, S.; Kottas, M.; et al. From Tropospheric Folding to Khamsin and Foehn Winds: How Atmospheric Dynamics Advanced a Record-Breaking Dust Episode in Crete. Atmosphere 2018, 9, 240. https://doi.org/10.3390/atmos9070240.

- Solomos, S.; Kallos, G.; Kushta, J.; Astitha, M.; Tremback, C.; Nenes, A.; Levin, Z. An integrated modeling study on the effects of mineral dust and sea salt particles on clouds and precipitation. Atmos. Chem. Phys. 2011, 11, 873–892.

- Solomos, S.; Spyrou, C.; Barreto, A.; Rodríguez, S.; González, Y.; Neophytou, M.K.A.; Mouzourides, P.; Bartsotas, N.S.; Kalogeri, C.; Nickovic, S.; Vimic A.V.; Mandic, M.V; Pejanovic, G.; Cvetkovic, B.; Amiridis, V.; Sykioti, O.; Gkikas, A.; Zerefos, C. The Development of METAL-WRF Regional Model for the Description of Dust Mineralogy in the Atmosphere. Atmosphere 2023, 14,1615. https://doi.org/10.3390/atmos14111615.

- Spyrou, C. Direct radiative impacts of desert dust on atmospheric water content. Aerosol Sci. Technol. 2018, 52, 693–701

- Spyrou, C., 2018: Direct radiative impacts of desert dust on atmospheric water content, Aerosol Science and Technology, 52:6, 693-701 DOI:10.1080/02786826.2018.1449940.

- Spyrou, C., Mitsakou, C., Kallos, G., Louka, P., and Vlastou, G. (2010). An Improved Limited Area Model for Describing the Dust Cycle in the Atmosphere. J. Geophys. Res., 115: D17211. doi:10.1029/2009JD013682.,

- Spyrou, C.; Kallos, G.; Mitsakou, C.; Athanasiadis, P.; Kalogeri, C.; Iacono, M.J. Modeling the radiative effects of desert dust on weather and regional climate. Atmos. Chem. Phys. 2013, 13, 5489–5504.

- Tewari, M., F. Chen, W. Wang, J. Dudhia, M. A. LeMone, K. Mitchell, M. Ek, G. Gayno, J. Wegiel, and R. H. Cuenca, 2004: Implementation and verification of the unified NOAH land surface model in the WRF model. 20th conference on weather analysis and forecasting/16th conference on numerical weather prediction, pp. 11–15.

- Thompson, Gregory, Paul R. Field, Roy M. Rasmussen, William D. Hall, 2008: Explicit Forecasts of Winter Precipitation Using an Improved Bulk Microphysics Scheme. Part II: Implementation of a New Snow Parameterization. Mon. Wea. Rev., 136, 5095–5115. doi:10.1175/2008MWR2387.1

- Toledano, C., Cachorro, V.E., Berjon, A., de Frutos, A.M., Sorribas, M., de la Morena, B.A. and Goloub, P. (2007), Aerosol optical depth and Ångström exponent climatology at El Arenosillo AERONET site (Huelva, Spain). Q.J.R. Meteorol. Soc., 133: 795-807. https://doi.org/10.1002/qj.54

- Ukhov, A., Ahmadov, R., Grell, G., and Stenchikov, G.: Improving dust simulations in WRF-Chem v4.1.3 coupled with the GOCART aerosol module, Geosci. Model Dev., 14, 473–493, https://doi.org/10.5194/gmd-14-473-2021, 2021.

- Zaveri, R. A., Easter, R. C., Fast, J. D., and Peters, L. K.: Model for simulating aerosol interactions and chemisty (MOSAIC), J. Geophys. Res., 113, D13204, doi:10.1029/2007JD008782, 2008.